Synthesis of MnO/cotton based carbon composites as lithium-ion battery anodes: a study on their structures and properties

Chenhao Zhao[1,2] ✉, *Ling Li*[1]

[1]*College of Chemistry and Materials, Longyan University, Fujian Longyan, People's Republic of China*
[2]*Fujian Provincial Key Laboratory of Clean Energy Materials, LongYan University, Fujian Longyan, People's Republic of China*
✉ *E-mail: 3514983317@qq.com*

Published in Micro & Nano Letters; Received on 27th September 2018; Revised on 3rd March 2019; Accepted on 12th March 2019

The construction of transition metal oxides/carbon composites has been one of the most useful methods to improve the electrochemical performances of transition metal oxides as anodes of lithium-ion batteries (LIBs). It has been found that various carbon amounts will make a great effect on the structures and properties of composites. In this work, the MnO/cotton based carbon composites are immediately obtained at an inert atmosphere from $Mn(NO_3)_2$–cotton mixture, which is readily produced based on the adsorption characteristic of cotton. The influences of carbon contents derived from various cotton amounts on the structures and electrochemical properties of MnO are studied. The results show that decreased crystallinity and improved porous properties can be achieved with increased carbon contents. As LIBs anodes, their electrochemical behaviours are distinct and deeply influenced by carbon contents. The MnO/cotton based carbon composite obtained at a cotton amount of 0.3 g delivers an initial reversible discharge capacity of 812.4 mAh g^{-1}, and a capacity of 775.9 mAh g^{-1} can be retained after 50 cycles. Meanwhile, the structure–function relation is also discussed in the text.

1. Introduction: Development of transition metal oxides (TMOs)/carbon composites as lithium-ion batteries (LIBs) anodes have been one of the hot topics in the recent decade [1–3]. Generally speaking, TMOs can deliver a high discharge capacity (600–1000 mAh g^{-1}). While they also encounter poor electronic conductivity and serious volume changes during cycling. In comparison, porous carbon with low discharge capacity possesses good electronic conductivity and flexible nature [4, 5]. As a result, the formation of TMOs/porous carbon composites can overcome the above shortages of TMOs, and an effect of '1 + 1 > 2' can be expected [6–8]. More importantly, the existence of carbon can inhibit the crystal growth of TMOs during preparation, as well as protect from pulverisation and aggregations of TMOs particle during charge–discharge process, which is essential for effective utilisation and cycling performance of anode materials [7, 9].

Besides the formation of composites with carbon, a selection of suitable TMOs is also important as LIBs anodes. Manganese-based oxides such as MnO, Mn_3O_4, Mn_2O_3 and spinel AMn_2O_4 (A = Zn, Co or Ni) have attracted numerous attentions due to their high discharge capacities and low costs especially low charge voltage compared with cobalt and iron based oxides [6–12]. For example, Wei *et al.* reported the synthesis of hollow MnO microcubes by topological transformation from hollow $MnCO_3$ microcubes. The hollow MnO microcubes revealed excellent electrochemical performance as LIB anodes. It could retain a discharge capacity of 914.6 mAh g^{-1} at 0.5 C even after 200 cycles [13]. In our previous work, a kind of hierarchical porous $ZnMn_2O_4$ fibre derived from cotton template also shows good electrochemical performance as LIBs anodes [14].

Furthermore, the synthesis of TMOs/porous carbon composites is another hot topic. Generally, an initial preparation, surface functionalisation of carbon substrate and subsequent combination with TMOs have been greatly improved [15, 16]. However, this route is a little time and energy consuming. Seeking for simple route is also very important. For example, Zhu *et al.* have prepared a MnO/carbon composites from a cotton directed route, and the composite show good electrochemical performance as LIBs anodes [17]. In this study, this facile route also has been further developed for the preparation of MnO/cotton based carbon composites. Importantly, by varying the amount of cotton, the influences of carbon contents on their structures and properties have been studied in the text.

2. Experimental

2.1. Synthesis of MnO/cotton based carbon composites: All of the reagents were A.R. grade and used without further purification. 1.7895 g of $Mn(NO_3)_2$ (50 wt% in solution) was added into a certain amount of distilled water. Then, x g (i.e. 0, 0.1, 0.3 and 0.5 g) of absorbent cotton was immersed into the above solution to ensure uniformly and sufficiently adsorb. After dried in an oven at 80°C overnight, the obtained cotton-metal nitrate composite was calcinated in a tube furnace at 600°C for 4 h with flowing argon [3, 7]. It should be mentioned that the added distilled water in the preparation of $Mn(NO_3)_2$ solution was ten times to the weight of cotton, which was to ensure the uniform and sufficient adsorption.

2.2. Structural characterisation: X-ray diffraction (XRD) patterns of the as-prepared composites were recorded in a powder X-ray diffractometer (DX-2700, Dandong) in a 2θ range from 10 to 80° with a scanning rate of 0.06°/s. Morphology, surface structure of each sample, was observed by scanning electron microscope (SEM, Hitachi S-3400) with Au coated pretreatment. Specific surface areas and pore structures of composites were calculated from N_2 adsorption–desorption isotherms, conducted in a Micromeritics Sorptometer (TriStar II 3020).

2.3. Electrochemical study: CR2016 coin cells were used throughout the experiments at room temperature. The working electrode was prepared as follows: 0.105 g of MnO/carbon composite, 0.03 g of acetylene black and 0.015 g of binder sodium alginate [18] were sufficiently mixed in an agate mortar, then pasted on the copper foil after forming slurry by adding the proper amount of water. After drying at 80°C overnight under air, the decorated copper foils were cut into a disc with a diameter of 14 mm, which was used as working electrode. Li plates (China Energy Lithium) were used as the counter and reference electrode.

Commercial LBC-301 purchased from ShenZhen CapChem and Celgard 2400 membrane were used as electrolyte and separator, respectively. The coin cells were assembled in an Ar-filled glove box. The discharge–charge tests were carried out in a CT-3008 battery test system (Shenzhen Neware) under a constant current mode in a voltage region between 0.01 and 3 V.

3. Results and discussion: In the experiment, the MnO/carbon composites are immediately prepared from $Mn(NO_3)_2$–cotton mixture. The adsorption characteristic of cotton can ensure the uniform contact between Mn ions and cotton, and subsequent MnO and cotton based carbon. Furthermore, the ratio between $Mn(NO_3)_2$ and cotton can be readily adjusted by changing cotton amounts.

The XRD patterns of MnO/carbon composites from different amounts of cotton are revealed in Fig. 1. The diffraction peaks of each sample can be indexed to the cubic-phase MnO (JCPDS Card No. 75–0257), without any impurities can be found, indicating the $Mn(NO_3)_2$ is transformed into MnO in the presence or absence of cotton. The diffraction peaks of graphite cannot be detected, suggesting the formation of amorphous carbon. Apparently, the intensities of diffraction peaks become weaker accompanying with the increased cotton amounts, which could be attributed to that high carbon content inhibits the crystallinity of MnO. In appearance, the colour of the as-prepared sample transforms from green (the colour of pure MnO) to dark green, and then black (the colour of carbon) with the increased cotton amounts.

The morphologies and surface microstructures of various MnO/carbon composites are revealed in Fig. 2. In the absence of cotton, the MnO presents an aggregation of nanoparticles, and the nanoparticles with clear corners and edges have an average size of several hundred nanometres (Fig. 2*a*). In the presence of 0.1 g cotton, the aggregation of MnO nanoparticles turns to be porous, which should be attributed to the partial template effect and decomposition of cotton.

When the cotton amount is increased to 0.3 g, an obvious fibre-like structure can be found (Fig. 2*c*), the size of this structure becomes to decades of micron. Some macropore exists on the surface of fibre. Interestingly, the MnO nanoparticles have not been found in a magnification view (Fig. 2*d*), suggesting an efficient combination with cotton-based carbon. The cotton is continuously elevated to 0.5 g, the fibre-like structure turns into more obvious (Fig. 2*e*), which should be the template effect of cotton. Unlike the surface porous structure (Fig. 2*d*), the MnO/carbon composite in Fig. 2*f* presents a crude surface, resulting from co-existence of a large amount of carbon.

Fig. 3 is the selected area and corresponding EDX spectrums, and it can be found that the amounts of carbon in the MnO/carbon composites are increased accompanying with the elevated cotton amounts, which is consistent with previous experimental design.

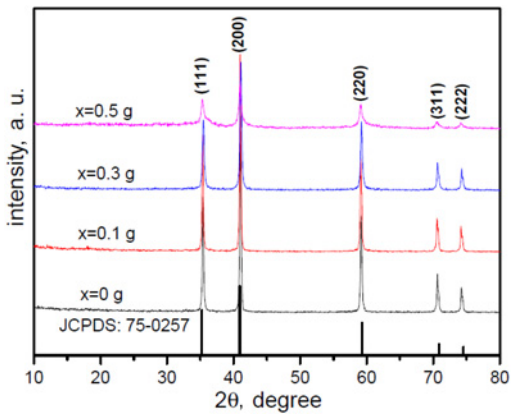

Fig. 1 *XRD patterns of MnO/carbon composites from different amounts of cotton*

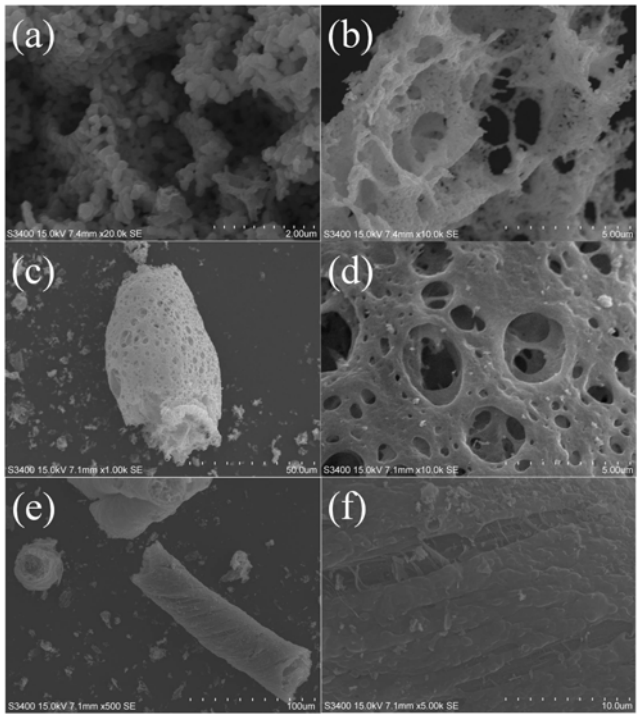

Fig. 2 *SEM images of MnO/carbon composites obtained in the presence of different cotton amounts*
a 0 g
b 0.1 g
c, *d* 0.3 g
e, *f* 0.5 g

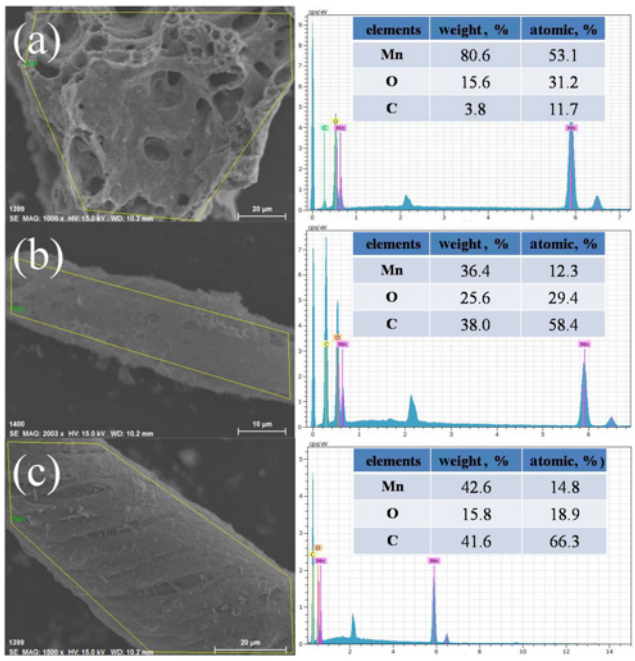

Fig. 3 *Selected area and EDX spectrums of MnO/carbon composites at different cotton amounts*
a 0.1 g
b 0.3 g
c 0.5 g

doi: 10.1049/mnl.2018.5596

Specific surface area and pore distribution are also important parameters for carbon-based composites. Fig. 4 is nitrogen adsorption–desorption isotherms and pore distribution of MnO/carbon composites. The calculated specific surface is 2.1, 5.1, 34.6 or 131.5 $m^2 g^{-1}$ at added cotton amounts of 0, 0.1, 0.3 or 0.5 g, respectively. It is obvious that the specific surface areas increase upon the elevated carbon contents. In the isotherms (Fig. 4*a*), a huge type H4 (horizontal arrangement) hysteresis loop can be found at the cotton amounts of 0.3 and 0.5 g, indicating the existence of meso-porous structures [19]. The pore distribution of each sample is shown in Fig. 4*b*, and the wide pore size in a range from tens to hundreds of nanometres can be presented, consisting of the SEM observation in Fig. 2*d*.

As we know, the electrochemical properties of MnO/carbon composites will be deeply determined by their structures. Fig. 5 shows the initial charge–discharge curves and cycling stability curves of various MnO/carbon at a current density of 0.2 A g^{-1}. An initial discharge capacity of 776.0, 1167.6, 1157.5 and 1364.4 mAh g^{-1}, and a reversible charge capacity of 455.1, 752.6, 807.6 or 901.0 mAh g^{-1} can be obtained for the samples of 0, 0.1, 0.3 or 0.5 g, respectively. Obviously, the reversible capacity increases with improved specific surface area, which should be attributed to that the elevated specific surface can provide more reaction site with electrolyte. Also, a voltage difference between charge and discharge processes can be clearly presented in Fig. 5*a*, and sample obtained at 0.5 g shows the lowest voltage difference, indicating it has a low inner resistance.

Cycling stabilities of various MnO/carbon composites at a current density of 0.2 A g^{-1} are revealed in Fig. 5*b*. The second cycle reversible capacities are 571.8, 742.9, 812.4 and 955.3 mAh g^{-1}, and values of 338.3, 562.7, 776.0 and 752.1 mAh g^{-1} can be retained after 50 cycles for the samples of 0, 0.1, 0.3 and 0.5 g, respectively, giving capacity retentions of 59.2, 75.7, 95.5 and 78.7%, respectively.

Interestingly, the situation of capacity evolution upon cycle is distinct among these samples. The bare MnO (i.e. $x = 0$ g sample) experiences a continuous decay in the discharge capacity upon

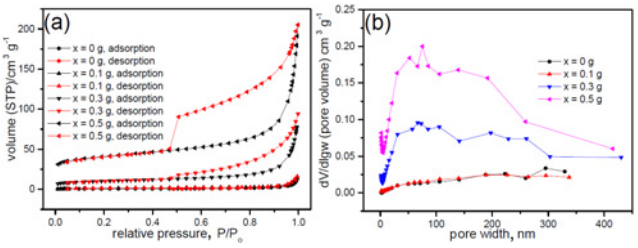

Fig. 4 *Specific surface areas and pore structures of different MnO/carbon composites*
a Nitrogen adsorption-desorption isotherms
b pore distribution

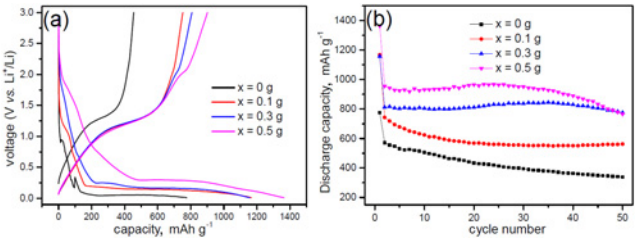

Fig. 5 *Electrochemical performances of various MnO/carbon composites at current density of 0.2 A g^{-1}*
a Initial charge-discharge curves
b Cycling stability

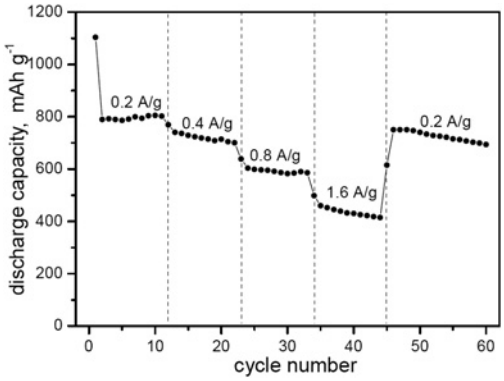

Fig. 6 *Rate capability of MnO/carbon obtained at a cotton amount of 0.3 g*

cycling. Consideration of its large particle size and low specific surface area, the volume change in charge–discharge process may destroy the crystal and particle structure, resulting in poor cycling stability [6, 7]. As for the sample obtained at 0.1 g cotton, it also encounters serious capacity decay in the beginning 10 cycles, and then keeps stable in the subsequent cycles, which is similar with widely reported TMOs [13, 14].

The other two samples with high carbon contents experience an initial increase on the discharge capacity, which should be attributed to the contribution of pseudocapacitive behaviours, and it is an interface energy storage behaviour related with the specific surface area of electrode material [20, 21], and a higher specific surface area means a higher intensity of interfacial energy storage. However, the pseudocapacitive contribution is unstable, and discharge capacities of the two electrodes begin to decay after dozens of cycles. Especially, the 0.5 g MnO/carbon composite encounters a serious capacity decrease after 30 cycles, also resulting from its high specific surface area and resultant side reaction with electrolyte.

After comparison, the MnO/carbon composite obtained from the cotton amount of 0.3 g is more suitable for LIB anode. Firstly, a moderate specific surface area (i.e. 34.6 $m^2 g^{-1}$) can provide sufficient reaction sites with electrolyte, and the side reaction also can be avoided compared with 0.5 g sample. Secondly, the carbon-containing MnO can inhibit the pulverisation and aggregations of TMOs particle during charge–discharge process, which is essential for the cycling stability of composite. Therefore, a rate capability study of MnO/carbon obtained at a cotton amount of 0.3 g is revealed in Fig. 6. The electrode undergoes a capacity decrease accompanying with an increased current density. In detail, a discharge capacity of 790.1, 708.5 or 598.9 mAh g^{-1} can be reached in a current density of 0.2, 0.4 or 0.8 A g^{-1}, respectively. When the current density is elevated to 1.6 A g^{-1}, a capacity value of 452.0 mAh g^{-1} can be reached. Unfortunately, the cycling stability in such a rate is not satisfied.

4. Conclusion: One-step cotton directed template route has been developed to synthesise MnO/carbon composites. The changed cotton amounts can produce different MnO/carbon composites, and resultant varying carbon contents will determine the structures and electrochemical properties of MnO/carbon composites as LIB anodes. A decreased crystallinity and improved specific surface area can be achieved with increased carbon contents. It has been found that an appropriate increase in the carbon content and porosity can improve the initial discharge capacity and cycling stability, while an excessive specific surface area (more than 100 $m^2 g^{-1}$) may be unsuitable to the cycling stability. A more clear work is necessary to explain the above phenomenon, deserved to be conducted continuously.

5. Acknowledgment: The authors thank the financial support from the Fujian Provincial IUI Cooperation Project (grant no. 2015H6016) and from the Provincial Science and Technology Department for Provincial Colleges and Universities Program (grant no. JK2015047).

6 References

[1] Qi W., Shapter J.G., Wu Q., *ET AL.*: 'Nanostructured anode materials for lithium-ion batteries: principle, recent progress and future perspectives', *J. Mater. Chem. A*, 2017, **5**, pp. 19521–19540

[2] Zhang J.J., Yu A.S.: 'Nanostructured transition metal oxides as advanced anodes for lithium-ion batteries', *Sci. Bull.*, 2015, **60**, pp. 823–838

[3] Li Y.J., Fan C.Y., Li H.H., *ET AL.*: '3D hierarchical microballs constructed by intertwined MnO@N-doped carbon nanofibers towards superior lithium-storage properties', *Chem. Eur. J.*, 2018, **24**, pp. 9606–9611

[4] Bai Q.H., Xiong Q.C., Li C.: 'Hierarchical porous carbons from a sodium alginate/bacterial cellulose composite for high-performance supercapacitor electrodes', *Appl. Surf. Sci.*, 2018, **455**, pp. 795–807

[5] Jia D.D., Yang Z.W., Zhang H., *ET AL.*: 'High performance of selenium cathode by encapsulating selenium into the micropores of chitosan-derived porous carbon framework', *J. Alloys Compd.*, 2018, **746**, pp. 27–35

[6] Huang S.Z., Zhang Q., Li Y., *ET AL.*: 'Grain boundaries enriched hierarchically mesoporous MnO/carbon microspheres for superior lithium ion battery anode', *Electrochim. Acta*, 2016, **222**, pp. 561–569

[7] Kang D.M., Liu Q.L., Si R., *ET AL.*: 'Crosslinking-derived MnO/carbon hybrid with ultrasmall nanoparticles for increasing lithium storage capacity during cycling', *Carbon*, 2016, **99**, pp. 138–147

[8] Tang X.M., Sui G., Cai Q., *ET AL.*: 'Novel MnO/carbon composite anode material with multi-modal pore structure for high performance lithium-ion batterie', *J. Mater. Chem. A*, 2016, **4**, pp. 2082–2088

[9] Zhang F.C., Wang Y., Guo W.B., *ET AL.*: 'Synthesis of Sn-MnO@nitrogen-doped carbon yolk-shelled three dimensional interconnected networks as a high-performance anode material for lithium-ion batteries', *Chem. Eng. J.*, 2019, **360**, pp. 1509–1516

[10] Zheng M.B., Tang H., Li L.L., *ET AL.*: 'Hierarchically nanostructured transition metal oxides for lithium-ion batteries', *Adv. Sci.*, 2018, **5**, p. 1700592

[11] Sekhar B.C., Kalaiselvi N.: 'Pristine hollow microspheres of Mn_2O_3 as a potential anode for lithium-ion batteries', *RSC Adv.*, 2015, **17**, pp. 5038–5045

[12] Zhang R.H., Hou L.R., Yuan C.Z.: 'Research progress of Mn-based mixed binary metal oxide anodes for lithium-ion battery', *Rare Met. Mater. Eng.*, 2016, **45**, pp. 1910–1916

[13] Wei Y.Y., Zi Z.F., Chen B.Z., *ET AL.*: 'Facile synthesis of hollow MnO microcubes as superior anode materials for lithium-ion batteries', *J. Alloys Compd.*, 2018, **756**, pp. 93–102

[14] Zhao C.H., Shen Y., Qiu S.E., *ET AL.*: 'Hierarchical porous $ZnMn_2O_4$ derived from cotton substance as high-performance lithium ion battery anode', *Micro Nano Lett.*, 2016, **11**, pp. 287–290

[15] Yao B., Ding Z.J., Feng X.Y., *ET AL.*: 'Enhanced rate and cycling performance of $FeCO_3$/graphene composite for high energy Li ion battery anodes', *Electrochim. Acta*, 2014, **148**, pp. 283–290

[16] Li P., Liu J.Y., Liu Y., *ET AL.*: 'Three-dimensional $ZnMn_2O_4$/porous carbon framework from petroleum asphalt for high performance lithium-ion battery', *Electrochim. Acta*, 2015, **180**, pp. 164–172

[17] Zhu C.Y., Han C.G., Saito G., *ET AL.*: 'Facile synthesis of MnO/carbon composites by a single-step nitratecellulose combustion synthesis for Li ion battery anode', *J. Alloys Compd.*, 2016, **689**, pp. 931–937

[18] Kovalenko I., Zdyrko B., Yushin G.: 'A major constituent of brown algae for use in high-capacity Li-ion batteries', *Science*, 2011, **334**, pp. 75–79

[19] Prahas D., Kartika Y., Indraswati N., *ET AL.*: 'Activated carbon from jackfruit peel waste by H_3PO_4 chemical activation: pore structure and surface chemistry characterization', *Chem. Eng. J.*, 2008, **140**, pp. 32–42

[20] Zhao S.Q., Feng F., Yu F.Q., *ET AL.*: 'Flower-to-petal structural conversion and enhanced interfacial storage capability of hydrothermally crystallized $MnCO_3$ via the in situ mixing of graphene oxide', *J. Mater. Chem. A*, 2015, **3**, pp. 24093–24102

[21] Feng F., Zhao S.Q., Liu R., *ET AL.*: 'Nio flowerlike porous hollow nanostructures with an enhanced interfacial storage capability for battery-to-pseudocapacitor transition', *Electrochim. Acta*, 2016, **222**, pp. 1160–1168

doi: 10.1049/mnl.2018.5596